Site-Directed Mutagenesis of the Catalytic Tryptophan Environment in *Pleurotus eryngii* Versatile Peroxidase[†,‡]

Francisco J. Ruiz-Dueñas,*[,§] María Morales,[§] María J. Mate,[§] Antonio Romero,[§] María Jesús Martínez,[§] Andrew T. Smith,[||] and Ángel T. Martínez*[,§]

Centro de Investigaciones Biológicas, CSIC, Ramiro de Maeztu 9, E-28040 Madrid, Spain, and Department of Biochemistry, School of Life Sciences, John Maynard Smith Building, University of Sussex, Falmer, Brighton BN1 9QG, U.K.

Received October 10, 2007; Revised Manuscript Received November 17, 2007

ABSTRACT: Lignin degradation by fungal peroxidases is initiated by one-electron transfer to an exposed tryptophan radical, a reaction mediated by veratryl alcohol (VA) in lignin peroxidase (LiP). Versatile peroxidase (VP) differs not only in its oxidation of Mn^{2+} at a second catalytic site but also in its ability to directly oxidize different aromatic compounds. The catalytic tryptophan environment was compared in LiP and VP crystal structures, and six residues near VP Trp164 were modified by site-directed mutagenesis. Oxidation of Mn^{2+} was practically unaffected. However, several mutations modified the oxidation kinetics of the high-redox-potential substrates VA and Reactive Black 5 (RB5), demonstrating that other residues contribute to substrate oxidation by the Trp164 radical. Introducing acidic residues at the tryptophan environment did not increase the efficiency of VP oxidizing VA. On the contrary, all variants harboring the R257D mutation lost their activity on RB5. Interestingly, this activity was restored when VA was added as a mediator, revealing the LiP-type behavior of this variant. Moreover, combination of the A260F and R257A mutations strongly increased (20−50-fold) the apparent second-order rate constants for reduction of VP compounds I and II by VA to values similar to those found in LiP. Dissociation of the enzyme−product complex seemed to be the limiting step in the turnover of this improved variant. Nonexposed residues in the vicinity of Trp164 can also affect VP activity, as found with the M247F mutation. This was a direct effect since no modification of the surrounding residues was found in the crystal structure of this variant.

Lignin removal, a key process for carbon recycling in land ecosystems as well as for industrial utilization of plant biomass (e.g., in paper pulp manufacturing or bioethanol production), is caused in nature by the action of wood-rotting fungi through a process that has been defined as enzymatic combustion (*1*). Several oxidoreductases secreted by ligninolytic basidiomycetes, the so-called white-rot fungi, are responsible for the first steps of lignin degradation in wood and other lignocellulosic materials, including enzymes from the groups of peroxidases, oxidases, and laccases (*2*, *3*). Ligninolytic peroxidases are the only enzymes described up to date that are able to break down model compounds representative of the main linkage types in lignin (such as nonphenolic β-*O*-4′ and β-1′ dimers) due to their high redox potential. Extracellular oxidases, such as glyoxal oxidase and aryl-alcohol oxidase, provide the hydrogen peroxide required by ligninolytic peroxidases. Finally, laccases can oxidize only phenolic units in lignin, although their oxidizing power is enhanced by redox mediators.

Ligninolytic hemeperoxidases from white-rot basidiomycetes include lignin peroxidases (LiPs),[1] manganese peroxidases (MnPs), and the more recently described versatile peroxidases (VPs) (*4*−*6*). Very recently, an extracellular heme-thiolate peroxidase has been found in some soil basidiomycetes that is also able to degrade lignin model compounds (*7*). LiP (EC 1.11.1.14) and MnP (EC 1.11.1.13) were first described in *Phanerochaete chrysosporium* and the genes and cDNA encoding isoenzymes LiPH8 and MnP1 cloned in 1987−1988 from the same fungus (*6*). From this date, up to 20 different genes from the *mnp* family and 12 genes from the *lip* family have been cloned from nine basidiomycete species (*8*). By contrast, VP has been described only in a few species from the genera *Pleurotus* and *Bjerkandera* (*9*−*12*). VP oxidizes Mn^{2+}, as MnP does (Mn^{3+} acting as a diffusible oxidizer of phenolic compounds and as a starter of lipid peroxidation), and high-redox-potential aromatic compounds, as LiP does. Due to their Mn-oxidizing

[†] This research was supported by Spanish Project BIO2005-03569 and EU Contract NMP2-CT-2006-026456 (BIORENEW). F.J.R.-D. thanks the EU for a project contract, and M.M. thanks CSIC for an I3P fellowship.

[‡] Atomic coordinates for native VP* have been deposited in the Protein Data Bank (entry 2BOQ).

* To whom correspondence should be addressed. Telephone: 34 918373112. Fax: 34 915360432. E-mail: FJRuiz@cib.csic.es or ATMartinez@cib.csic.es.

[§] CSIC.

[||] University of Sussex.

[1] Abbreviations: ABTS, 2,2′-azinobis(3-ethylbenzothiazoline-6-sulfonate); HRP, horseradish peroxidase; k_{obs}, pseudo-first-order rate constant; k_{app}, apparent second-order rate constant; k_{cat}, catalytic constant; K_D, equilibrium dissociation constant; K_m, Michaelis constant; LiP, lignin peroxidase; MnP, manganese peroxidase; PCR, polymerase chain reaction; PDB, Protein Data Bank; RB5, Reactive Black 5; rmsd, root-mean-square deviation; VA, veratryl alcohol; VP, versatile peroxidase; VPI, compound I of VP; VPII, compound II of VP.

10.1021/bi7020298 CCC: $40.75
Published on Web 01/18/2008

activity, the *Pleurotus* VP isoenzymes were first described as MnP isoenzymes (*13*, *14*), but they were later recognized as representing a new peroxidase type (EC 1.11.1.16). VP is also able to efficiently oxidize different phenolic compounds and low-redox-potential dyes that are the substrates of generic peroxidases (EC 1.11.1.7), such as nonligninolytic peroxidase from the soil basidiomycete *Coprinopsis cinerea* (synonym *Coprinus cinereus*) or horseradish peroxidase (HRP). Moreover, VP directly oxidizes high-redox-potential aromatic compounds and dyes that LiP oxidizes only in the presence of redox mediators (*15*−*18*).

The versatile catalytic properties of *Pleurotus eryngii* VP (isoenzymes VPL and VPS1) are due to a hybrid molecular architecture that includes in the same protein different catalytic sites for oxidation of Mn^{2+} and high-redox-potential aromatic substrates, related to those found in the MnP and LiP crystal structures (*19*, *20*). The Mn^{2+} oxidation site in VP has a higher plasticity than that of *P. chrysosporium* MnP, as shown by crystallographic and kinetic studies (*21*). On the other hand, the oxidation of high-redox-potential aromatic substrates and lignin model compounds is produced by long-range electron transfer (LRET) to heme from a tryptophanyl radical at the surface of LiP (*22*−*25*) and VP (*26*, *27*). It has been shown that the corresponding residue in LiP (Trp171) is β-hydroxylated during the first enzyme turnover (*19*, *28*), whereas this is not the case in VP (*27*). Moreover, residues surrounding the catalytic tryptophan are not conserved in LiP and VP, a fact that could explain differences in the kinetic constants for oxidation of aromatic substrates by these peroxidases. Differences in the tryptophan environment could also be related to the involvement of redox mediators, such as veratryl (3,4-dimethoxybenzyl) alcohol (VA) or dimethoxybenzenes, in LiP oxidation of some recalcitrant compounds that are directly oxidized by VP (*15*, *29*, *30*).

In this study, six amino acid residues, located in the vicinity of the catalytic tryptophan (Trp164) in the *P. eryngii* VP crystal structure, were modified by site-directed mutagenesis. The variants obtained were characterized in terms of their steady-state and transient-state kinetics for oxidation of VA, the most typical LiP substrate, and Reactive Black 5 (RB5), a high-redox-potential dye that is not oxidized by LiP in the absence of mediators. The kinetic results obtained were discussed together with crystallographic data to explain some of the peculiarities of substrate oxidation at the catalytic tryptophan of VP.

MATERIALS AND METHODS

Heterologous Expression. Native (nonmutated) recombinant VP (VP*) protein and different site-directed variants were expressed in *Escherichia coli* (*31*). The cDNA encoding the sequence of mature isoenzyme VPL (allelic variant VPL2; GenBank entry AF007222) (*10*) was cloned in expression vector pFLAG1 (International Biotechnologies Inc.), and plasmid pFLAG1-VPL2 was used for site-directed mutagenesis. *E. coli* DH5α was used for plasmid propagation, whereas *E. coli* W3110 was used for native and mutated cDNA expression. The VP* proteins obtained were activated in vitro and purified as indicated below.

Site-Directed Mutagenesis. Mutations were introduced by polymerase chain reaction (PCR), using expression plasmid pFLAG1-VPL2 as a template, and the QuikChange kit from Stratagene. For each mutation, both a direct and a reverse primer were designed complementary to opposite strands of the same DNA region.

The following primers were used for the different variants (only direct constructions, with indication of the changed triplets in bold, and the mutations introduced underlined): (i) S158D, 5′-GGGTGACGGCTTC**GAC**CCCGTCGAGGTTGTTTGGC-3′; (ii) S158E, 5′-GGGTGACGCAGGCTTC**GAG**CCCGTCGAGGTTGTTTGGC-3′; (iii) M247F, 5′-GCCTGCGAATGGCAGTCC**TTC**GTTAACAACCAACCG-3′; (iv) M247L, 5′-GCCTGCGAATGGCAGTCC**TTG**GTTAACAACCAACCG-3′; (v) R257D, 5′-CAACCGAAGATTCAGAAC**GAT**TTCGCTGCTACCATGTCG-3′; (vi) R257L, 5′-CAACCGAAGATTCAGAAC**CTT**TTCGCTGCTACCATGTCG-3′; (vii) R257K, 5′-CCAACCGAAGATTCAGAAC**AAG**TTCGCTGCTACCATGTCGAAG-3′; (viii) A260F, 5′-CGAAGATTCAGAACCGTTTCGCT**TTC**ACCATGTCGAAGATGGC-3′; (ix) K264A, 5′-GCTGCTACCATGTCG**GCG**ATGGCTCTTCTTGGC-3′; (x) R257A/A260F double variant, 5′-CGAAGATTCAGAAC**GCT**TTCGCT**TTT**ACCATGTCGAAGATGGCTCTTCTTGGC-3′. The double mutant S158E/R257D was obtained using plasmid pFLAG1-VPL2 (S158E) as a template and direct and reverse oligonucleotides as primers. The triple mutant N256D/R257D/A260F was obtained using plasmid pFLAG1-VPL2 (A260F) as a template and primers corresponding to the following oligonucleotide and its reverse: 5′-CAACCAACCGAAGATTCAG**GAC**GAT-TTCGCT**TTC**ACCATGTCG-3′. The mutated genes were completely sequenced using an ABI 3730 DNA analyzer (Applied Biosystem) to ensure that only the desired mutations were introduced.

PCRs (50 μL final volume) were carried out in a Perkin-Elmer Gene Amp PCR System 240 using 10 ng of template DNA, each dNTP at 500 μM, 125 ng of direct and reverse primers, 2.5 units of *Pfu*Turbo polymerase (Stratagene), and the manufacturer's buffer. Reaction conditions were as follows: (i) a "hot start" at 95 °C for 1 min; (ii) 18 cycles at 95 °C for 50 s, 55 °C for 50 s, and 68 °C for 10 min; and (iii) a final cycle at 68 °C for 10 min.

Enzyme Production, in Vitro Activation, and Purification. Native VP* and site-directed variants were produced in *E. coli* W3110 after transformation with the corresponding plasmids. Cells were grown for 3 h in Terrific Broth, induced with 1 mM isopropyl β-D-thiogalactopyranoside, and grown for a further 4 h. The apoenzyme accumulated in inclusion bodies, as shown by sodium dodecyl sulfate−polyacrylamide gel electrophoresis, and was recovered using 8 M urea. Subsequent in vitro folding was performed using 0.16 M urea, 5 mM Ca^{2+}, 20 μM hemin, 0.5 mM oxidized glutathione, 0.1 mM dithiothreitol, and 0.1 mg/mL protein, at pH 9.5 (*31*). Active enzyme was purified by Resource-Q chromatography using a 0 to 0.3 M NaCl gradient (2 mL/min, 20 min) in 10 mM sodium tartrate (pH 5.5) containing 1 mM $CaCl_2$.

Spectroscopic Measurements. Electronic absorption spectra were recorded at 25 °C using a Shimadzu UV-160 spectrophotometer. The concentrations of native VP* and site-directed variants were calculated from the absorption at 407 nm using an extinction coefficient of 150 mM^{-1} cm^{-1} (*10*). For spectroscopic characterization of the transient states in

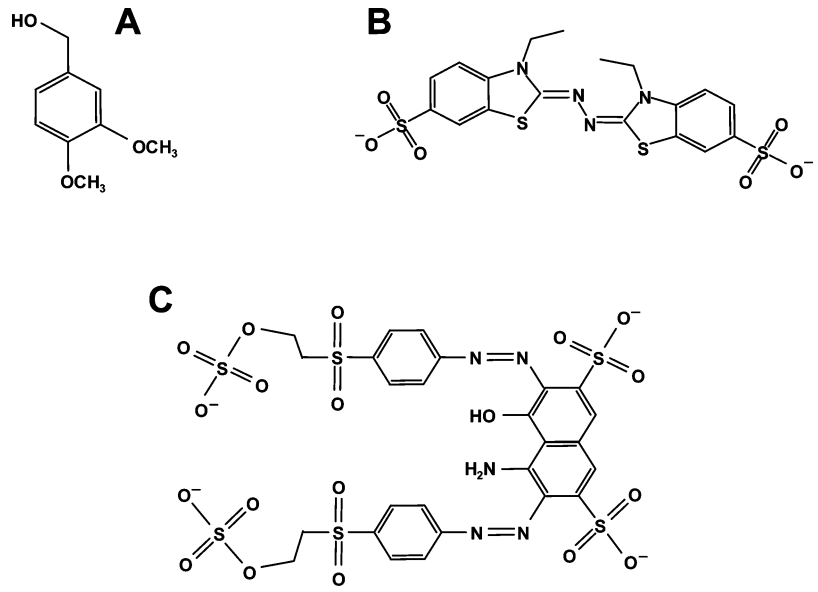

FIGURE 1: Chemical structures of VA (A), ABTS (B), and RB5 (C) used as VP substrates.

VP catalytic cycle, 1 equiv of H_2O_2 was added to the resting enzyme in 10 mM sodium tartrate (pH 5) yielding compound I. Addition of 1 equiv of ferrocyanide to compound I yielded compound II.

Steady-State Enzyme Kinetics. Mn-independent oxidation of VA (veratraldehyde $\epsilon_{310} = 9300\ M^{-1}\ cm^{-1}$) was estimated at pH 3.0, and those of RB5 ($\epsilon_{598} = 30000\ M^{-1}\ cm^{-1}$) and 2,2′-azinobis(3-ethylbenzothiazoline-6-sulfonate) (ABTS; cation radical $\epsilon_{436} = 29300\ M^{-1}\ cm^{-1}$) were estimated at pH 3.5. The chemical structures of the substrates mentioned above are shown in Figure 1. Direct oxidation of Mn^{2+} was estimated by the formation of the Mn^{3+}•tartrate complex ($\epsilon_{238} = 6500\ M^{-1}\ cm^{-1}$) using 0.1 M sodium tartrate (pH 5). All enzymatic activities were measured as initial velocities taking linear increments (decreases in the case of RB5) at 25 °C in the presence of 0.1 mM H_2O_2. Steady-state kinetic constants were calculated from oxidation of increasing substrate concentrations. Mean values and standard errors for apparent affinity constant (Michaelis constant, K_m) and maximal enzyme turnover (catalytic constant, k_{cat}) were obtained by nonlinear least-squares fitting of the experimental measurements to the Michaelis−Menten model. Fitting of these constants to the normalized equation $v = (k_{cat}/K_m)[S]/(1 + [S]/K_m)$ yielded the efficiency values (k_{cat}/K_m) with their corresponding standard errors.

Transient-State Enzyme Kinetics. Transient-state kinetic constants were measured at 25 °C, or 10 °C when required, using stopped-flow equipment (Bio-Logic) including a three-syringe module (SFM300) synchronized with a diode array detector (J&M), and Bio-Kine software. Compound I formation was investigated by mixing the resting enzyme with increasing concentrations of H_2O_2 in 100 mM sodium tartrate (pH 3) under pseudo-first-order conditions (excess of substrate) and followed at 397 nm (the isosbestic point of VP compounds I and II). To investigate compound II formation, compound I was first prepared by mixing 4 μM resting enzyme with 1 equiv of H_2O_2 in 10 mM sodium tartrate (pH 5). After the sample had aged for 0.6 s in a delay line, an excess of substrate in 100 mM (final concentration) sodium tartrate [pH 3 (VA) or pH 3.5 (RB5)] was added, and compound II formation was followed at 416 nm (the isosbestic point of VP compound II and resting enzyme). The first step in investigating compound II reduction consisted of production and reduction of compound I by premixing a solution of 4 μM enzyme and 4 μM ferrocyanide with 1 equiv of H_2O_2 in 10 mM sodium tartrate (pH 5). The mixture was incubated for 6 s in the delay line, and compound II reduction was followed at 406 nm (the Soret maximum of the resting enzyme) after mixing with different concentrations of VA or RB5 in 100 mM (final concentration) sodium tartrate (pH 3 for VA and pH 3.5 for RB5). In all cases, the final concentration of enzyme was 1 μM. All kinetic traces exhibited single-exponential character from which pseudo-first-order rate constants were calculated.

Crystal Structure. The crystal structure of VP* expressed in *E. coli* was recently determined by K. Piontek (Albert-Ludwigs University, Freiburg, Germany) and deposited as Protein Data Bank (PDB) entry 2BOQ. Crystals of the M247F variant were obtained by the hanging drop vapor diffusion method. The protein (10 mg/mL) was mixed 1:1 with a solution containing 1.4 M ammonium sulfate and 100 mM sodium cacodylate (pH 5.0). The crystals appeared after 29 days, and to improve the quality, they were seeded on freshly equilibrated drops using a microprobe. Then, they were flash-cooled in a cryosolution containing the crystallization medium and 25% glycerol. A complete data set was collected at beamline ID14.2 of ESRF (Grenoble, France). Data reduction was done using MOSFLM and SCALA, from the CCP4 package. The structure was determined by molecular replacement using MOLREP and the native VP* (allelic variant VPL2) crystal model (PDB entry 2BOQ) as a search probe. Consecutive cycles of refinement and manual rebuilding were conducted using REFMAC and COOT. The statistics of data collection, processing, and refinement are given in Table 1. Figures were produced using Pymol and Swiss-PdbViewer.

RESULTS

Catalytic Tryptophan Environment. Figure 2A shows the position of the side chains of nine amino acid residues from helices F, I, and J in the vicinity of the catalytic tryptophan (Trp164) of VP, and the corresponding residues in LiP

Table 1: Data Collection, Processing, and Refinement Statistics of the VP* (Isoenzyme VPL) M247F Variant Crystal Structure

space group	*I*41	R_{cryst}/R_{free} (%)	14.4 (18.6)[a]
unit-cell *a* (Å)	96.29	Ramachandran plot	
unit-cell *b* (Å)	96.29	preferred regions (%)	96.76
unit-cell *c* (Å)	98.53	allowed regions (%)	3.24
resolution range (Å)	2.0	rmsd	
completeness (%)	99.3 (98.8)[a]	bonds (Å)	0.020
R_{mean} (%)	14.5 (47.3)[a]	angles (deg)	1.65
I/σ	10.7 (3.3)[a]		

[a] Values in parentheses correspond to the last resolution shell of 2.11−2.00 Å.

(Figure 2B), as found in the crystal structures of both enzymes. As shown in panels C and D of Figure 2, eight of these residues are at the surface of the enzyme around the indole side chain of the catalytic tryptophan and, therefore, could be responsible for the differences in binding and oxidation of high-redox-potential substrates by these two peroxidases. The two conformations of the Arg257 side chain found in VP* crystal structures (Figure 2A) are both exposed to the solvent, although only one of them is shown in Figure 2C. The absence of a benzenic side chain near the exposed tryptophan (as found in LiP) increases the accessibility to the catalytic tryptophan in VP, where Ala260 occupies the position of LiP Phe267. In addition to topological differences, surface charge distribution around the catalytic tryptophan strongly differs between VP and LiP. Five exposed acid residues are present in LiP, namely, Asp165, Glu168, Glu250, Asp263, and Asp264, the former being substituted with Ser158 in VP and the latter two with Asn256 and Arg257, respectively. In addition to Arg257, a second basic residue, Lys264, is exposed in the environment of the catalytic tryptophan of VP (the homologous residue in LiP being Ala271).

Site-Directed Mutagenesis of Amino Acid Residues in the Trp164 Environment of VP. Among the residues mentioned above, VP Glu161, Trp164, Glu243, and Lys253 are conserved in LiP (as Glu168, Trp171, Glu250, and Lys260, respectively), and therefore, they were not mutated in VP. The other six residues were modified by PCR site-directed mutagenesis substituting them with those present in LiP (S158D, M247F, N256D, R257D, A260F, and K264A mutations) in several single or multiple variants. Five

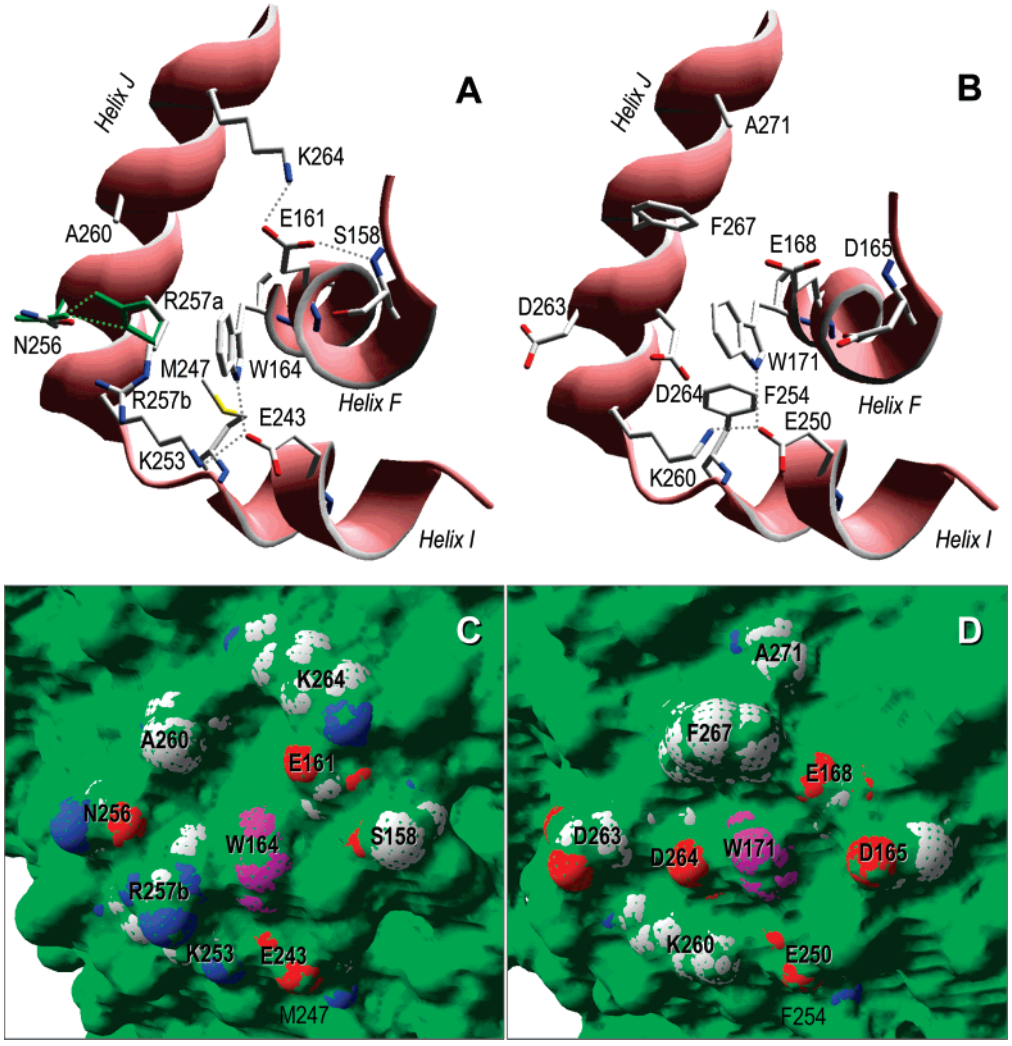

FIGURE 2: Catalytic tryptophan environments in the crystal structures of VP (left) and LiP (right). (A and B) Amino acid side chains from helices F, I, and J around Trp164 of native VP [Ser158, Glu161, Glu243, Met247, Lys253, Asn256, Arg257, Ala260, and Lys253 (A)] and Trp171 of native LiP [Asp165, Glu168, Glu250, Phe254, Lys260, Asp263, Asp264, Phe267, and Ala271 (B)]. Two dispositions of the VP Arg257 side chain are included, and several H-bonds (<3 Å) are indicated. **(**C and D) Solvent access surfaces (green) and exposed residues (CPK colors) around the catalytic tryptophan (magenta) of VP (C) and LiP (D) (residues as van der Waals spheres). From PDB entries 2BOQ (VP, isoenzyme VPL) and 1LGA (LiP, isoenzyme LiPH8).

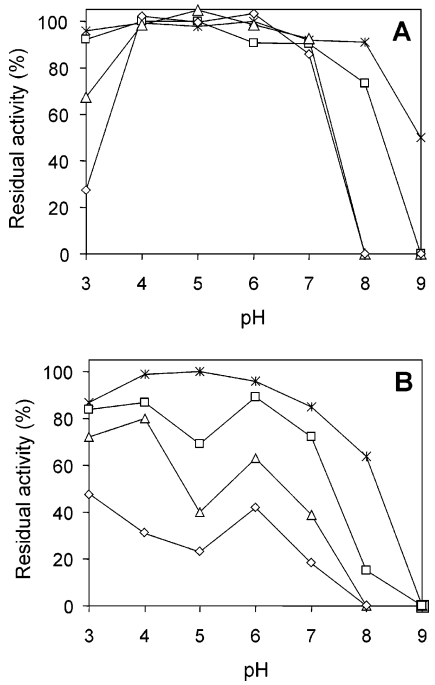

FIGURE 3: Comparison of the pH stability of native VP* (A) and its R257D (B) variant after incubation for 0 (∗), 1 (□), 24 (△), and 96 h (◇) at 4 °C in citrate/phosphate/borate buffer (pH 3−9). Residual activities were measured using Mn^{2+} as a substrate at pH 5 and expressed as percentages of the initial activity.

additional mutations, including other amino acid residues (S158E, M247L, R257L, R257K, and R257A substitutions), were also introduced. The electronic absorption spectra of the different variants obtained were similar to those of native VP*, including resting-state characteristic maxima at 407, 505, and 637 nm, confirming that no changes in the heme environment had been produced as a result of the substitutions introduced into the Trp164 environment.

Substitution of Arg257 with an aspartate residue, as found in LiP, strongly decreased the stability of the resulting variant compared with native VP*. Whereas native VP* was stable for 96 h at 4 °C in the pH range of 4−7, the residual activity of the R257D variant decreased with incubation time over the whole pH range (Figure 3). Therefore, the information on variants including the R257D mutation was limited: some of them could not be successfully refolded or yielded a very small amount of active enzyme (N256D/R257D/A260F triple variant), and others were too unstable for stopped-flow and crystallographic studies (R257D), or even for steady-state kinetic studies (S158E/R257D double variant).

When helix J was rebuilt by changing two more residues (VP Asn256 and Ala260) to those present in LiP, the enzyme stability was improved. These VP* stabilization effects are being investigated in more detail.

Steady-State Kinetics of VP Site-Directed Variants. The steady-state kinetic constants for oxidation of four different substrates (VA, RB5, ABTS, and Mn^{2+}) by native VP* and 11 single or multiple variants are listed in Table 2. None of the mutations caused important changes in VP* oxidation of Mn^{2+}, in agreement with the existence of a different binding site for this metal cation. By contrast, substitution of Trp164 eliminated the ability of VP* to oxidize VA and RB5, as expected from the direct involvement of this amino acid residue in oxidation of high-redox-potential aromatic substrates. High-affinity oxidation of ABTS was simulta-

Table 2: Steady-State Kinetic Constants of Native VP* (Isoenzyme VPL) and Single and Multiple Variants [K_m (μM), k_{cat} (s^{-1}), and k_{cat}/K_m ($mM^{-1}\ s^{-1}$)] for Oxidation of VA, RB5, ABTS, and Mn^{2+} [a]

		VP*	W164S[b]	S158D	S158E	R257D	R257L
VA	K_m	4130 ± 320	−[d]	5690 ± 20	1650 ± 20	54700 ± 4700	13500 ± 600
	k_{cat}	9.5 ± 0.2	0	9.6 ± 0.1	9.6 ± 0.1	19.6 ± 1.0	27.3 ± 0.5
	k_{cat}/K_m	2.3 ± 0.1	0	1.7 ± 0.0	5.9 ± 0.1	0.4 ± 0.0	2.0 ± 0.0
RB5	K_m	3.4 ± 0.3	−[d]	1.4 ± 0.1	2.2 ± 0.2	−[d]	2.7 ± 0.2
	k_{cat}	5.5 ± 0.3	0	4.9 ± 0.1	4.6 ± 0.1	0	11.6 ± 0.3
	k_{cat}/K_m	1610 ± 90	0	3620 ± 250	2090 ± 120	0	4310 ± 230
ABTS[c]	K_m	3.0 ± 0.2	−[d]	4.0 ± 0.2	2.8 ± 0.2	nd[e]	1.7 ± 0.1
	k_{cat}	8.1 ± 0.2	0	7.7 ± 0.2	9.1 ± 0.3	nd[e]	22.2 ± 0.3
	k_{cat}/K_m	2700 ± 140	0	1900 ± 80	3300 ± 200	nd[e]	12950 ± 850
Mn^{2+}	K_m	181 ± 10	110	182 ± 16	204 ± 12	71 ± 6	102 ± 9
	k_{cat}	275 ± 4	207	144 ± 4	350 ± 4	111 ± 3	100 ± 2
	k_{cat}/K_m	1520 ± 70	1900	792 ± 56	1720 ± 90	1560 ± 100	982 ± 76

		R257K	A260F	K264A	M247F	M247L	R257A/ A260F
VA	K_m	14200 ± 1000	5110 ± 500	5680 ± 300	4110 ± 400	6990 ± 630	13500 ± 1200
	k_{cat}	10.9 ± 0.3	7.5 ± 0.2	8.2 ± 0.2	4.3 ± 0.2	5.0 ± 0.2	17.9 ± 0.7
	k_{cat}/K_m	0.8 ± 0.0	1.5 ± 0.1	1.4 ± 0.1	1.1 ± 0.1	0.7 ± 0.0	1.3 ± 0.1
RB5	K_m	2.6 ± 0.2	1.9 ± 0.1	2.5 ± 0.2	3.1 ± 0.2	1.3 ± 0.0	4.9 ± 0.5
	k_{cat}	2.3 ± 0.1	3.1 ± 0.1	4.2 ± 0.1	0.4 ± 0.0	3.3 ± 0.0	9.1 ± 0.4
	k_{cat}/K_m	890 ± 55	1600 ± 100	1650 ± 110	122 ± 5	2580 ± 40	1900 ± 100
ABTS	K_m	3.6 ± 0.2	9.0 ± 0.5	6.5 ± 0.3	3.5 ± 0.2	2.6 ± 0.1	3.2 ± 0.2
	k_{cat}	11.8 ± 0.3	5.9 ± 0.2	8.8 ± 0.2	0.7 ± 0.0	4.9 ± 0.1	18.6 ± 0.3
	k_{cat}/K_m	3300 ± 100	700 ± 25	1300 ± 44	200 ± 6	1910 ± 60	5700 ± 300
Mn^{2+}	K_m	75 ± 7	72 ± 5	60 ± 3	70 ± 5	82 ± 7	150 ± 8
	k_{cat}	95 ± 2	144 ± 2	134 ± 2	76 ± 1	150 ± 4	207 ± 3
	k_{cat}/K_m	1270 ± 90	2000 ± 110	2240 ± 100	1090 ± 70	1830 ± 130	1380 ± 60

[a] Reactions at 25 °C in 0.1 M tartrate (pH 3 for VA, pH 3.5 for RB5 and ABTS, and pH 5 for Mn^{2+}). Means and 95% confidence limits. [b] VA, RB5, and Mn^{2+} constants from Pérez-Boada et al. (*27*). [c] A second K_m for ABTS could be obtained in the millimolar range (all variants). [d] Not determined because of a lack of activity. [e] Not determined.

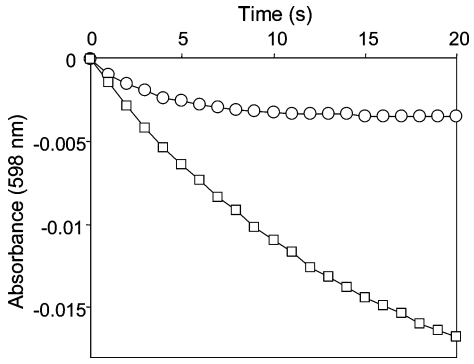

FIGURE 4: VA-mediated decolorization of RB5 by the R257D VP* variant (□) compared with absence of decolorization when VA was not included in the reaction mixture (○). Reactions at 25 °C in 100 mM sodium tartrate (pH 3.5) using 20 μM RB5, 25 mM VA (in the VA-mediated reaction), 0.1 mM H_2O_2, and 0.04 μM enzyme.

neously suppressed, although this low-redox-potential dye was still oxidized at a low-affinity site characterized by a K_m of ~1 mM (data not shown).

The efficiency of VP* in oxidizing VA was also decreased by Arg257 mutations (83% decrease in the R257D variant, 65% decrease in the R257K variant, and 43% decrease in the R257A/A260F variant). Changes in oxidation of RB5 were simultaneously caused by these mutations (including complete loss of activity in the R257D and S158E/R257D variants), as well as by the M247F substitution (92% efficiency decrease). Moreover, the unstable S158E/R257D variant was completely unable to oxidize RB5, and the low-refolding-yield N256D/R257D/A260F variant did not oxidize RB5 or VA (kinetic constants for other substrates not included).

The low efficiency of the Arg257 variants oxidizing VA was mainly due to a decrease in the apparent substrate affinity (up to 13-fold increase in K_m for the R257D variant). In contrast, the effect of the M247F mutation on RB5 and ABTS oxidation was mainly due to a decrease in activity (91−93% decrease in k_{cat}), whereas the apparent affinity was not affected.

As shown in Figure 4, which presents the results of the RB5 decolorization assay by the R257D variant in the absence and presence of VA, this variant was unable to directly oxidize RB5, as the native VP* did, but its activity was restored in the presence of VA. However, VA did not stimulate RB5 oxidation by the M247F variant. On the contrary, addition of VA inhibited RB5 oxidation by this variant, as well as by native VP*.

Transient-State Kinetics of VP Site-Directed Variants. Kinetic constants for formation and reduction of the transient states of the VP catalytic cycle (*27*), the so-called compound I (VPI) and compound II (VPII), were determined using VA and RB5 as reducing substrates (S) that were oxidized to S_{ox} (eqs 1−3). With this purpose, stopped-flow spectrophotometry of native VP* and the W164S, M247F, R257A/A260F, A260F, R257L, and R257K variants was performed. As explained above, those variants including the R257D mutation were too unstable for stopped-flow experiments.

$$VP + H_2O_2 \rightarrow VPI + H_2O \quad (1)$$

$$VPI + S \rightarrow VPII + S_{ox} \quad (2)$$

$$VPII + S + 2H^+ \rightarrow VP + S_{ox} + H_2O \quad (3)$$

The observed pseudo-first-order rate constants from the kinetic traces of compound I formation (k_{1obs}) exhibited a linear dependence of the H_2O_2 concentration passing through the origin. Fitting k_{1obs} versus H_2O_2 concentration to a straight line yielded slope values corresponding to the apparent second-order rate constant for compound I formation (k_{1app}). The similar k_{1app} values obtained for native VP* and site-directed variants (Table 3) indicated that the mutations did not affect formation of compound I by H_2O_2. These values (~3 μM^{-1} s^{-1}) were on the same order of magnitude found for MnP and higher than those found in LiP.

Transient-State Kinetics: Compound I Reduction. The kinetic traces for one-electron reduction of compound I by VA and RB5 exhibited single-exponential character from which the pseudo-first-order rate constants (k_{2obs}) were calculated. Plots of k_{2obs} versus RB5 concentration were linear (Figure 5A), and apparent second-order rate constants (k_{2app}) were determined as the slope of a second-order plot. By contrast, plots of k_{2obs} versus VA concentration exhibited both saturation (Figure 5B) and nonsaturation kinetics (Figure 5C) depending on the VP* variant. Apparent second-order rate constants for those VP* variants showing nonsaturation kinetics were determined as described for RB5. When saturation kinetics were observed, first-order rate (k_2) and equilibrium dissociation constants (K_{D2}) for reduction of compound I by VA could be calculated according to eqs 4−6 (Figure 5B). The apparent second-order rate constant k_{2app} (k_2/K_{D2}) for these variants was estimated by a nonlinear

Table 3: Transient-State Kinetic Constants of VP* Variants Compared with Those of Native VP* (Isoenzyme VPL)[a]

		RB5		VA	
	k_{1app}	k_{2app}	k_{3app}	k_{2app}	k_{3app}
VP*	3460 ± 70	3880 ± 80	1150 ± 70	2.8 ± 0.1	1.33 ± 0.07
W164S	3840 ± 60	230 ± 15	−[d]	0.056 ± 0.006	−[d]
M247F	4200 ± 40	7090 ± 550	540 ± 190	4.04 ± 0.17	3.77 ± 0.25
R257A/A260F	3300 ± 150	≈30000[b]	3390 ± 25	61.6 ± 0.5	67.9 ± 17.0
A260F	3270 ± 90	5600 ± 300	800 ± 100	12.0 ± 1.2	4.47 ± 0.4
R257K	3360 ± 60	3340 ± 200	990 ± 50	6.4 ± 0.5	1.75 ± 0.17
R257L	2950 ± 90	nd[c]	nd[c]	nd[c]	6.87 ± 0.41

[a] Apparent second-order rate constants (mM^{-1} s^{-1}) of formation of compound I (k_{1app}) by H_2O_2 and reduction of compounds I (k_{2app}) and II (k_{3app}) by RB5 or VA. Reactions at 25 °C in 100 mM sodium tartrate (pH 3.5 for RB5 and pH 3 for VA) using 1 μM VP*, final concentrations, conducted as described in the text. Means and 95% confidence limits of replicate assays. [b] Estimated at 10 °C. [c] Not determined. [d] Not determined because of a lack of activity.

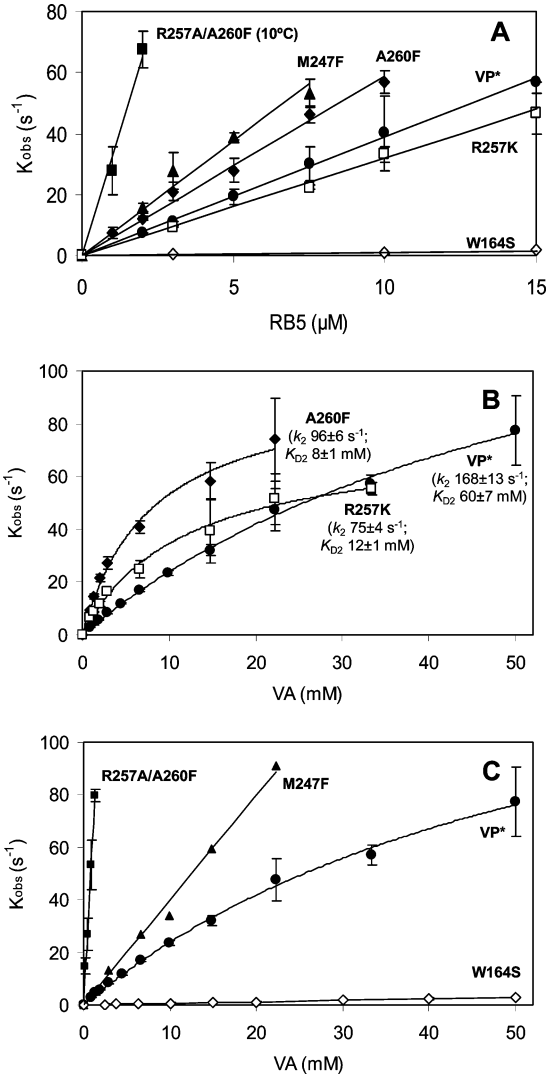

FIGURE 5: Kinetics of reduction of compound I of native VP* (●) and the W164S (◇), M247F (▲), R257K (□), A260F (◆), and R257A/A260F (■) variants. (A) Reduction by RB5 (all variants). (B) Reduction by VA of those variants exhibiting saturation kinetics (first-order rate constants, k_2, and equilibrium dissociation constants, K_{D2}, in parentheses). (C) Reduction by VA of those variants exhibiting nonsaturation kinetics (compared with that of native VP*). Reduction of R257A/A260F compound I by RB5 was followed at 10 °C (because it was too fast at higher temperatures), but all the other reactions were assessed at 25 °C. The reaction mixtures contained 1 μM enzyme and 100 mM tartrate (pH 3 for VA and pH 3.5 for RB5). All kinetic traces displayed single-exponential character and were fitted to obtain k_{obs} values. Means and 95% confidence limits of replicate assays are shown.

least-squares fit to eq 5 adapted as follows: $k_{2obs} = (k_2/K_{D2})\cdot[VA]/(1 + [VA]/K_{D2})$.

$$VPI + VA \overset{K_{D2}}{\rightleftharpoons} VPI{-}VA \overset{k_2}{\rightleftharpoons} VP{-}VA^{\bullet+} \rightleftharpoons VP + VA^{\bullet+} \quad (4)$$

$$K_{2obs} = k_2/(1 + K_{D2}/[VA]) \quad (5)$$

$$K_{D2} = ([VPI][VA])/[VPI{-}VA] \quad (6)$$

Interestingly, the k_{2app} values for compound I reduction by both substrates (Table 3) increased in the M247F, A260F, and R257A/A260F variants with respect to that of native VP*. The increases were especially noticeable for the R257A/A260F variant, reaching 61.6 mM^{-1} s^{-1} for VA and a very high value around 30000 mM^{-1} s^{-1} for RB5 (the last value estimated at 10 °C because the reaction was too fast at 25 °C). A large decrease (94−98%) in k_{2app} was observed for RB5 and VA reduction of compound I of the variant bearing a mutation at the catalytic tryptophan (W164S). The improvement in the reduction of R257K and A260F compound I by VA was due to a decrease in K_{D2} (5- and 7.5-fold, respectively).

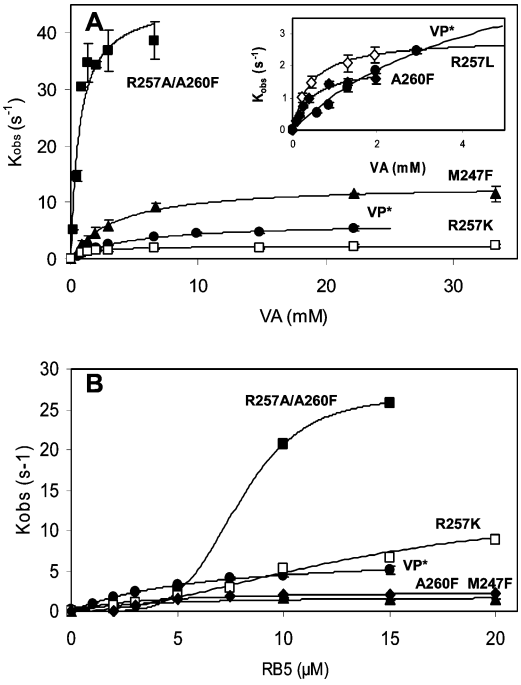

FIGURE 6: Kinetics of reduction of compound II by VA (A) and RB5 (B): native VP* (●), M247F (▲), R257K (□), R257L (◇), A260F (◆), and R257A/A260F (■). All kinetic traces displayed single-exponential character and were fitted to obtain k_{obs} values. Means and 95% confidence limits of replicate assays are shown. Reactions were carried out at 25 °C using 1 μM enzyme and 100 mM tartrate (pH 3 for VA and pH 3.5 for RB5).

Transient-State Kinetics: Compound II Reduction. Pseudo-first-order rate constants for one-electron reduction of compound II by VA and RB5 (k_{3obs}) were estimated. Plots of k_{3obs} versus VA concentration exhibited a hyperbolic behavior (as found for reduction of compound I of native VP*), the rates saturating with an increase in substrate (S) concentration (Figure 6A). Compound II reduction can be explained by eqs 7−9, k_3 and K_{D3} being its first-order rate constant and equilibrium dissociation constant, respectively. The apparent second-order rate constants of compound II reduction, k_{3app} (k_3/K_{D3}), were calculated by a nonlinear least-squares fit to eq 8 adapted as follows: $k_{3obs} = (k_3/K_{D3})[S]/(1 + [S]/K_{D3})$.

$$VPII + S \overset{K_{D3}}{\rightleftharpoons} VPII{-}S \overset{k_3}{\rightleftharpoons} VP{-}S_{ox} \rightleftharpoons VP + S_{ox} \quad (7)$$

$$k_{3obs} = k_3/(1 + K_{D3}/[S]) \quad (8)$$

$$K_{D3} = ([VPII][S])/[VPII{-}S] \quad (9)$$

Plots of k_{3obs} versus RB5 concentration exhibited two different behaviors (Figure 6B): (i) hyperbolic for native VP* and the A260F and M247F variants (as found for

Table 4: Comparison of Transient-State Kinetic Constants for Reduction of Compound II of VP* (Isoenzyme VPL) Variants by RB5 or VA[a]

	RB5		VA	
	k_3	K_{D3}	k_3	K_{D3}
VP*	7.3 ± 0.3	0.0064 ± 0.0007	6.5 ± 0.2	4.88 ± 0.39
W164S	–[b]	–[b]	0.22 ± 0.06	nd[c]
M247F	1.9 ± 0.2	0.0035 ± 0.0016	13.2 ± 0.4	3.50 ± 0.30
R257A/A260F	26.8 ± 0.3	0.0079 ± 0.0001	45.9 ± 4.5	0.67 ± 0.22
A260F	2.6 ± 0.1	0.0033 ± 0.0004	2.1 ± 0.1	0.46 ± 0.05
R257K	13.6 ± 1.1	0.0136 ± 0.0016	2.3 ± 0.1	1.3 ± 0.1
R257L	nd[c]	nd[c]	2.9 ± 0.1	0.42 ± 0.03

[a] First-order rate constants (k_3, s^{-1}) and equilibrium dissociation constants (K_{D3}, mM). Reactions at 25 °C in 100 mM sodium tartrate (pH 3.5 for RB5 and pH 3 for VA) using 1 μM VP*, final concentration, conducted as described in the text. Means and 95% confidence limits of replicate assays. [b] Not determined because of a lack of activity. [c] Not determined.

reduction of compound II by VA), k_3, K_{D3}, and k_{3app} being calculated according to eqs 7−9, and (ii**)** sigmoidal for the R257K and R257A/A260F variants, the data being rationalized using the Hill equation $k_{3obs} = k_3/(1 + K_{0.5}/[S]^n)$, where $K_{0.5}$ is the substrate concentration at which the velocity is half-maximal (which was considered equivalent to K_{D3} in this work) and n is the Hill coefficient. The sigmoidal plots observed for reduction of compound II of the latter variants suggested two binding sites for oxidation of RB5, as found for other VP substrates (*8*, *15*). One of them corresponds to the Trp164 environment, and its improvement (k_3 increase) in the R257A/A260F variant would explain the observed behavior; on the other hand, the second one could also be located near Trp164 or at a different region of the VP surface.

As found for k_{2app}, k_{3app} was also increased by some of the mutations that were introduced (Table 3). The increase was especially high, more than 50-fold, for reduction of compound II of the R257A/A260F variant by VA. The k_3 for reduction of W164S compound II by VA (Table 4) decreased to a value (0.22 s^{-1}) that was in the same range of the self-reduction rate of native VP*. By contrast, the double mutation R257A/A260F strongly improved the k_3 constant for both VA (7-fold increase) and RB5 (4-fold increase), and a simultaneous improvement in the K_{D3} for VA was observed (7-fold decrease). Improvement of the VA K_{D3} (11-fold lower value) was also observed for the A260F and R257L variants, although a simultaneous increase in k_3 was not produced. Finally, the M247F mutation resulted in a 2-fold increase in the k_3 constant for VA, but it simultaneously caused a 4-fold decrease in RB5 k_3 (whereas the K_{D3} constants for both substrates were barely modified).

Comparison of Steady-State and Transient-State Kinetic Constants. For native VP*, the values of VA K_{D3} (4.9 mM) and k_3 (6.5 s^{-1}) were in agreement with the steady-state K_m (4.1 mM) and k_{cat} (9.5 s^{-1}) constants, respectively, indicating that compound II reduction is the limiting step at full saturation in the VP catalytic cycle, and the same happened for the RB5 constants. However, this was not the case for some of the variants, such as R257A/A260F that had VA K_{D3} (0.67 mM) and k_3 (45.9 s^{-1}) values significantly improved with respect to the corresponding K_m (13.5 mM) and k_{cat} (17.9 s^{-1}) constants, respectively. This inconsistency suggests formation of an enzyme−product complex (after compound II reduction). In native VP*, reduction of compound II would be the limiting step in enzyme turnover (k_{3app} being similar to k_{cat}/K_m). However, after strongly improving the rates of reduction of compounds I and II by the R257A/A260F double mutation, dissociation of the enzyme−product complex would be the limiting step (resulting in a k_{cat}/K_m ratio similar to that of native VP*, in spite of the 50-fold increase in k_{3app}).

Crystallographic Studies. The native VP* crystal structure has recently been determined at 1.3 Å resolution. The M247F variant was also crystallized and its structure determined at 2.0 Å. A detail of the electron density map is shown in Figure 7, corresponding to the catalytic Trp164 and six neighbor residues, including Arg257, that showed two equally probable side chain conformations (the heme group is observed behind). The M247F model includes residues 1−317, the heme prosthetic group, two Ca^{2+} ions, two sulfate ions, and water molecules. The overall structures of the native VP* and the M247F variant were very similar. The C_α root-mean-square deviation (rmsd) was 0.36 Å, and the few residues that showed a high rmsd (residues 74, 224, 289−291, and 296) are located in exposed loops and involved in crystallographic contacts. The mutated protein displayed the same global fold as the native one, with 11 α-helices and four disulfide bridges. Around the mutation there were not big conformational changes, and the main chain of the mutated residue formed the same hydrogen bonds as in the native structure. The phenylalanine side chain was almost in the same place as the side chain of the native methionine residue, i.e., located in a hydrophobic cavity lined by Val163, Trp164, Ala167, Phe198, Glu243, Trp244, Ile254, and the basic chains of Lys253 and Arg257. The Arg257 side chain, which displayed a double conformation, was also in the same two positions found in the native structure.

DISCUSSION

VA in Fungal Degradation of Lignin. It has been suggested that VA plays a central role in lignin degradation by *P. chrysosporium* and other basidiomycetes (*32*). In addition to protecting LiP against hydrogen peroxide inactivation, VA is required for efficient oxidation of different aromatic compounds and dyes by LiP. These include simple phenols (*33*), monomethoxylated aromatics (*29*), polymeric dyes, including Poly R-478 (*34*), polycyclic aromatic hydrocarbons (*35*), high-redox-potential dyes (*15*), ferricytochrome *c* (*36*), and, most importantly, polymeric lignin (*37*). In most cases, VA acts as a redox mediator via the cation radical ($VA^{\bullet+}$) formed by one-electron abstraction by LiP. Aromatic cation radicals are also produced by other LiP mediators, such as simple and substituted dimethoxybenzenes (*29*, *30*). The short lifetime of the $VA^{\bullet+}$ radical (around 60 ms, at pH 3) prevents its free diffusion from the enzyme to the lignin macromolecule and suggested that the mediating action should be produced as an enzyme-bound species (*38*). Then, it has been shown that the LiP-bound $VA^{\bullet+}$ radical was stabilized and decayed more slowly than the free radical in bulk solution, and it has been proposed that the stabilization may be due to the acidic microenvironment in the enzyme active site (*24*, *39*). Finally, evidence of the formation of a $VA^{\bullet+}$ radical bound to LiP has been obtained by EPR (*40*).

In contrast to LiP, VP of *Pleurotus* and *Bjerkandera* species does not require redox mediators to oxidize simple

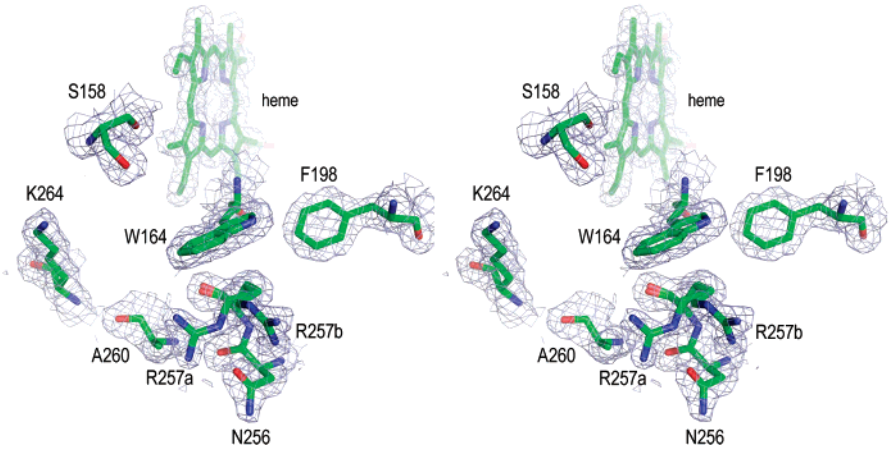

FIGURE 7: Stereoview of a representative ($2F_o - F_c$) electron density map of the M247F variant, contoured at the 1.5σ level, showing the catalytic Trp164 of VP and neighbor Ser158, Phe198, Asn256, Arg257, Ala260, and Lys264, including the double position (a and b) of the Arg257 side chain.

phenols or high-redox-potential dyes, including RB5 (*15*), as well as polycyclic aromatic hydrocarbons (*18*), polymeric dyes (*16*), and lignin (*41*, *42*). Interestingly, whereas VA is the main aromatic metabolite secreted by *P. chrysosporium* (*43*), the fungi from the genera *Pleurotus* and *Bjerkandera* produce *p*-anisaldehyde involved in H_2O_2 generation (*44*), without a significant production of VA (*45*, *46*).

Aromatic Substrate Oxidation Sites in VP and LiP. A crystal structure of LiP or VP containing VA or other aromatic compound has not been reported yet. However, when the LiP crystal structure was determined for the first time, it was assumed that LiP substrates would be oxidized at the same place found for other peroxidases (e.g., HRP), and VA was modeled at the heme access channel (*32*, *47*). The existence of this hypothetical oxidation site in direct contact with the heme conditioned the first reaction mechanisms proposed for VA-mediated oxidation of lignin by LiP (*48*).

However, in spite of several conflicting results (*49*) and some molecular dynamics studies showing the plasticity of the heme access channel (*50*), it is currently assumed that VA oxidation is produced by LRET from a tryptophan residue at the surface of *P. chrysosporium* LiP (*24*), and VP from *Pleurotus* (*16*, *27*) and *Bjerkandera* species (*17*). Moreover, it has been shown that MnP can be engineered for VA oxidation by introducing a tryptophan residue homologous to the LiP and VP catalytic tryptophan (*51*), and the same strategy has been proposed for improving other peroxidases (*52*).

The site mentioned above was identified in the crystal structure of VP, and the involvement of some amino acid residues in the vicinity of the catalytic Trp164 is discussed below. The characteristics of the catalytic tryptophan environment would be at the origin of some of the differences in high-redox-potential substrate oxidation by ligninolytic peroxidases, e.g., the lack of LiP activity on RB5 in contrast with VP, the lower-VP-efficiency oxidizing VA, and the VA-mediated activity of LiP on some substrates that VP can oxidize directly.

Introducing Acidic Residues into the Trp164 Environment: R257D Variant with VA-Mediated Activity. It has been suggested that a partially acidic environment of Trp171 in *P. chrysosporium* LiP would stabilize the $VA^{\bullet+}$ radical to act as an enzyme-bond mediator (*40*). Recently, it has been demonstrated that three of the exposed acid residues also affected the kinetics of VA oxidation by LiP (*52*). Two acid residues in the Trp171 environment of LiP (Glu168 and Glu250) are conserved in VP, and three others were introduced here as single and/or multiple VP* mutations.

In contrast with the initial expectations that suggested a more efficient oxidation of VA as found in LiP, the N256D/R257D/A260F variant completely lost its activity on VA. Moreover, this triple variant as well as the R257D and S158E/R257D variants also lost their activity on RB5. Interestingly, the RB5 oxidizing activity of the R257D variant was restored via addition of VA to the reaction mixture. The behavior of the R257D variant of VP is similar to the VA-mediated activity of LiP on RB5 and other substrates, as discussed above, and contrasted with the direct oxidation of this dye by native VP (*15*).

A VP Variant (R257A/A260F) Exhibiting LiP-Type Transient-State Kinetics. The apparent second-order rate constants of the R257A/A260F variant revealed much more efficient reduction of both compounds I and II by VA (more than 20- and 50-fold improvement, respectively) and RB5 (7- and 3-fold improvement, respectively) than native VP. Moreover, the first-order rate and dissociation constants for reduction of its compound II evidenced improvement of both the k_3 and K_{D3} constants for VA. Comparison of the VA steady-state and transient-state kinetic constants for this double variant pointed to formation of an enzyme−product complex, whose dissociation rate would be the limiting step in enzyme turnover, once the substrate oxidation rates by both compounds I and II had been strongly improved due to the mutations that were introduced.

It is noteworthy that the k_{3app} for reduction of compound II of the VP R257A/A260F variant by VA (68 mM^{-1} s^{-1}) was only slightly lower than that reported for *P. chrysosporium* LiP (185 mM^{-1} s^{-1}), and its k_3 (46 s^{-1}) was even higher than that of the latter peroxidase (34 s^{-1}) (*25*). The single A260F and R257L variants also showed some decreases in VA K_{D3}, but the k_3 values were not comparable to that obtained for the double variant, indicating that the simultaneous removal of Arg257 and incorporation of a phenylalanine residue (homologous to LiP Phe267) are

required to produce a VP variant with VA transient-state kinetic constants comparable to those of LiP.

Topological and Kinetic Considerations on Substrate (VA and RB5) Oxidation by VP and LiP. The most outstanding characteristic of the LiP surface near Trp171 is the protruding side chain of Phe267 in an environment with a partial negative charge. On the other hand, the VP crystal structure showed several basic residues in the environment of Trp164, including Arg257 and Lys264, and an alanine residue (Ala260) at the position of LiP Phe267.

We initially considered that the lack of LiP activity on RB5 compared to VP could be related to the presence of Phe267 interrupting the transversal furrow where this large substrate would be accommodated near the catalytic tryptophan of VP. However, this does not seem to be the case since introduction of a phenylalanine residue (A260F VP variant) did not strongly modify the VP kinetic constants for RB5. In contrast, VP activity on RB5 was eliminated by the R257D mutation (alone or in combination with other changes). Therefore, it is suggested that the lack of RB5 oxidation by LiP is not due to steric hindrances (by the Phe267 side chain) but to the existence of a partially negative environment (including Asp264 which is homologous to VP Arg257, and Asp165 which is homologous to VP Ser158) compared with the positively charged environment of VP Trp164 (including Lys264 in addition to Arg257) that would favor binding and oxidation of RB5 and other anionic substrates.

Oxidation of RB5 (and ABTS) by VP is also affected by some nonexposed residues, as shown by the steady-state kinetic constants of the M247F variant. The k_{cat} decreases (more than 90%) suggested that the introduction of the phenylalanine residue in the vicinity of Trp164 affects the electron transfer from the substrates mentioned above. The changes in VP activity were due to only the exchange of this amino acid residue and not to structural modifications affecting the surrounding residues, as revealed by the crystal structure of the variant compared with that of the native enzyme.

With regard to VA oxidation, it is interesting that not only the double R257A/A260F mutation, the unique catalytic properties of which were discussed above, but also the A260F and R257L single mutations (and not the R257K mutation) improved the VP* K_{D3} constant for VA. This indicated that the insertion of a benzenic side chain or the removal of a basic side chain at these positions improves binding of VA on VP. It is at least curious how two so different substitutions yielded variants with a similarly improved kinetic constant. We can hypothesize that the R257L mutation would facilitate the direct interaction between VA and Trp164, whereas the A260F mutation would promote binding between VA and the phenylalanine ring (by aromatic−aromatic interactions). The remarkable additive effect of simultaneously removing Arg257 and introducing a phenylalanine residue at position 260 of VP, which increased the k_3 of the resulting R257A/A260F variant to a value higher than found in LiP (*25*), indicated that a better binding or orientation of VA in the catalytic site improves not only substrate binding but also the compound II reduction rate.

Finally, the VA-mediated oxidation of RB5 by the VP* variant incorporating the R257D mutation (which exhibited a LiP-type behavior) suggested stabilization of the $VA^{\bullet+}$ radical by a more acidic (less basic) Trp164 environment, more similar to that found around the catalytic tryptophan of LiP that has been related to the VA-mediated activity of this peroxidase on different substrates (*40*).

ACKNOWLEDGMENT

We acknowledge the European Synchrotron Radiation Facility, and Joanna Timmis for assistance in using beamline ID14.2. Klaus Piontek (Albert-Ludwigs University, Freiburg, Germany) is acknowledged for providing access to the crystal structure of native VP*.

REFERENCES

1. Kirk, T. K., and Farrell, R. L. (1987) Enzymatic "combustion": The microbial degradation of lignin, *Annu. Rev. Microbiol. 41*, 465−505.
2. Martínez, A. T., Speranza, M., Ruiz-Dueñas, F. J., Ferreira, P., Camarero, S., Guillén, F., Martínez, M. J., Gutiérrez, A., and del Río, J. C. (2005) Biodegradation of lignocellulosics: Microbiological, chemical and enzymatic aspects of fungal attack to lignin, *Int. Microbiol. 8*, 195−204.
3. Kersten, P., and Cullen, D. (2007) Extracellular oxidative systems of the lignin-degrading Basidiomycete *Phanerochaete chrysosporium*, *Fungal Genet. Biol. 44*, 77−87.
4. Gold, M. H., Youngs, H. L., and Gelpke, M. D. (2000) Manganese peroxidase, *Met. Ions Biol. Syst. 37*, 559−586.
5. Martínez, A. T. (2002) Molecular biology and structure-function of lignin-degrading heme peroxidases, *Enzyme Microb. Technol. 30*, 425−444.
6. Cullen, D., and Kersten, P. J. (2004) Enzymology and molecular biology of lignin degradation, in *Mycota.III: Biochemistry and Molecular Biology* (Brambl, R., and Marzluf, G. A., Eds.) 2nd ed., pp 249−273, Springer, Berlin.
7. Hofrichter, M., and Ullrich, R. (2006) Heme-thiolate haloperoxidases: Versatile biocatalysts with biotechnological and environmental significance, *Appl. Microbiol. Biotechnol. 71*, 276−288.
8. Ruiz-Dueñas, F. J., Aguilar, A., Martínez, M. J., Zorn, H., and Martínez, A. T. (2007) Gene cloning, heterologous expression, *in vitro r*econstitution and catalytic properties of a versatile peroxidase, *Biocatal. Biotransform. 25*, 276−285.
9. Camarero, S., Sarkar, S., Ruiz-Dueñas, F. J., Martínez, M. J., and Martínez, A. T. (1999) Description of a versatile peroxidase involved in natural degradation of lignin that has both Mn-peroxidase and lignin-peroxidase substrate binding sites, *J. Biol. Chem. 274*, 10324−10330.
10. Ruiz-Dueñas, F. J., Martínez, M. J., and Martínez, A. T. (1999) Molecular characterization of a novel peroxidase isolated from the ligninolytic fungus *Pleurotus eryngii*, *Mol. Microbiol. 31*, 223−236.
11. Mester, T., and Field, J. A. (1998) Characterization of a novel manganese peroxidase-lignin peroxidase hybrid isozyme produced by *Bjerkandera* species strain BOS55 in the absence of manganese, *J. Biol. Chem. 273*, 15412−15417.
12. Moreira, P. R., Duez, C., Dehareng, D., Antunes, A., Almeida-Vara, E., Frère, J. M., Malcata, F. X., and Duarte, J. C. (2005) Molecular characterisation of a versatile peroxidase from a *Bjerkandera* strain, *J. Biotechnol. 118*, 339−352.
13. Giardina, P., Palmieri, G., Fontanella, B., Rivieccio, V., and Sannia, G. (2000) Manganese peroxidase isoenzymes produced by *Pleurotus ostreatus* grown on wood sawdust, *Arch. Biochem. Biophys. 376*, 171−179.
14. Martínez, M. J., Ruiz-Dueñas, F. J., Guillén, F., and Martínez, A. T. (1996) Purification and catalytic properties of two manganese-peroxidase isoenzymes from *Pleurotus eryngii*, *Eur. J. Biochem. 237*, 424−432.
15. Heinfling, A., Ruiz-Dueñas, F. J., Martínez, M. J., Bergbauer, M., Szewzyk, U., and Martínez, A. T. (1998) A study on reducing substrates of manganese-oxidizing peroxidases from *Pleurotus eryngii* and *Bjerkandera adusta*, *FEBS Lett. 428*, 141−146.
16. Kamitsuji, H., Watanabe, T., Honda, Y., and Kuwahara, M. (2005) Direct oxidation of polymeric substrates by multifunctional manganese peroxidase isozyme from *Pleurotus ostreatus* without redox mediators, *Biochem. J. 386*, 387−393.

17. Tinoco, R., Verdín, J., and Vázquez-Duhalt, R. (2007) Role of oxidizing mediators and tryptophan 172 in the decoloration of industrial dyes by the versatile peroxidase from *Bjerkandera adusta*, *J. Mol. Catal. B: Enzym. 46*, 1−7.
18. Wang, Y. X., Vázquez-Duhalt, R., and Pickard, M. A. (2003) Manganese-lignin peroxidase hybrid from *Bjerkandera adusta* oxidizes polycyclic aromatic hydrocarbons more actively in the absence of manganese, *Can. J. Microbiol. 49*, 675−682.
19. Blodig, W., Smith, A. T., Doyle, W. A., and Piontek, K. (2001) Crystal structures of pristine and oxidatively processed lignin peroxidase expressed in *Escherichia coli* and of the W171F variant that eliminates the redox active tryptophan 171. Implications for the reaction mechanism, *J. Mol. Biol. 305*, 851−861.
20. Sundaramoorthy, M., Youngs, H. L., Gold, M. H., and Poulos, T. L. (2005) High-resolution crystal structure of manganese peroxidase: Substrate and inhibitor complexes, *Biochemistry 44*, 6463−6470.
21. Ruiz-Dueñas, F. J., Morales, M., Pérez-Boada, M., Choinowski, T., Martínez, M. J., Piontek, K., and Martínez, A. T. (2007) Manganese oxidation site in *Pleurotus eryngii* versatile peroxidase: A site-directed mutagenesis, kinetic and crystallographic study, *Biochemistry 46*, 66−77.
22. Mester, T., Ambert-Balay, K., Ciofi-Baffoni, S., Banci, L., Jones, A. D., and Tien, M. (2001) Oxidation of a tetrameric nonphenolic lignin model compound by lignin peroxidase, *J. Biol. Chem. 276*, 22985−22990.
23. Blodig, W., Smith, A. T., Winterhalter, K., and Piontek, K. (1999) Evidence from spin-trapping for a transient radical on tryptophan residue 171 of lignin peroxidase, *Arch. Biochem. Biophys. 370*, 86−92.
24. Doyle, W. A., Blodig, W., Veitch, N. C., Piontek, K., and Smith, A. T. (1998) Two substrate interaction sites in lignin peroxidase revealed by site-directed mutagenesis, *Biochemistry 37*, 15097−15105.
25. Gelpke, M. D. S., Lee, J., and Gold, M. H. (2002) Lignin peroxidase oxidation of veratryl alcohol: Effects of the mutants H82A, Q222A, W171A, and F267L, *Biochemistry 41*, 3498−3506.
26. Pogni, R., Baratto, M. C., Teutloff, C., Giansanti, S., Ruiz-Dueñas, F. J., Choinowski, T., Piontek, K., Martínez, A. T., Lendzian, F., and Basosi, R. (2006) A tryptophan neutral radical in the oxidized state of versatile peroxidase from *Pleurotus eryngii*: A combined multi-frequency EPR and DFT study, *J. Biol. Chem. 281*, 9517−9526.
27. Pérez-Boada, M., Ruiz-Dueñas, F. J., Pogni, R., Basosi, R., Choinowski, T., Martínez, M. J., Piontek, K., and Martínez, A. T. (2005) Versatile peroxidase oxidation of high redox potential aromatic compounds: Site-directed mutagenesis, spectroscopic and crystallographic investigations of three long-range electron transfer pathways, *J. Mol. Biol. 354*, 385−402.
28. Blodig, W., Doyle, W. A., Smith, A. T., Winterhalter, K., Choinowski, T. H., and Piontek, K. (1998) Autocatalytic formation of hydroxy group at Cβ of Trp171 in lignin peroxidase, *Biochemistry 37*, 8832−8838.
29. Harvey, P. J., Schoemaker, H. E., and Palmer, J. M. (1986) Veratryl alcohol as a mediator and the role of radical cations in lignin biodegradation by *Phanerochaete chrysosporium*, *FEBS Lett. 195*, 242−246.
30. Teunissen, P. J. M., and Field, J. A. (1998) 2-Chloro-1,4-dimethoxybenzene as a mediator of lignin peroxidase catalyzed oxidations, *FEBS Lett. 439*, 219−223.
31. Pérez-Boada, M., Doyle, W. A., Ruiz-Dueñas, F. J., Martínez, M. J., Martínez, A. T., and Smith, A. T. (2002) Expression of *Pleurotus eryngii* versatile peroxidase in *Escherichia coli* and optimisation of *in vitro* folding, *Enzyme Microb. Technol. 30*, 518−524.
32. Schoemaker, H. E., Lundell, T. K., Hatakka, A. I., and Piontek, K. (1994) The oxidation of veratryl alcohol, dimeric lignin models and lignin by lignin peroxidase: The redox cycle revisited, *FEMS Microbiol. Rev. 13*, 321−332.
33. Koduri, R. S., and Tien, M. (1995) Oxidation of guaiacol by lignin peroxidase. Role of veratryl alcohol, *J. Biol. Chem. 270*, 22254−22258.
34. Harvey, P. J., Candeias, L. P., King, P. J., Palmer, J. M., and Wever, R. (1995) Lignin peroxidase catalysis: Reaction with veratryl alcohol and a polymeric dye, Poly R, *Biochem. Soc. Trans. 23*, S340.
35. Barr, D. P., and Aust, S. D. (1994) Mechanisms white rot fungi use to degrade pollutants, *Environ. Sci. Technol. 28*, A78−A87.
36. Sheng, D., and Gold, M. H. (1998) Irreversible oxidation of ferricytochrome *c* by lignin peroxidase, *Biochemistry 37*, 2029−2036.
37. Hammel, K. E., Jensen, K. A., Mozuch, M. D., Landucci, L. L., Tien, M., and Pease, E. A. (1993) Ligninolysis by a purified lignin peroxidase, *J. Biol. Chem. 268*, 12274−12281.
38. Candeias, L. P., and Harvey, P. J. (1995) Lifetime and reactivity of the veratryl alcohol radical cation: Implications for lignin peroxidase catalysis, *J. Biol. Chem. 270*, 16745−16748.
39. Khindaria, A., Yamazaki, I., and Aust, S. D. (1996) Stabilization of the veratryl alcohol cation radical by lignin peroxidase, *Biochemistry 35*, 6418−6424.
40. Khindaria, A., Nie, G., and Aust, S. D. (1997) Detection and characterization of the lignin peroxidase compound II−veratryl alcohol cation radical complex, *Biochemistry 36*, 14181−14185.
41. Camarero, S., Bocchini, P., Galletti, G. C., Martínez, M. J., and Martínez, A. T. (2001) Compositional changes of wheat lignin by a fungal peroxidase analyzed by Pyrolysis-GC/MS, *J. Anal. Appl. Pyrolysis 58/59*, 413−423.
42. Moreira, P. R., Almeida-Vara, E., Malcata, F. X., and Duarte, J. C. (2007) Lignin transformation by a versatile peroxidase from a novel *Bjerkandera* sp strain, *Int. Biodeterior. Biodegrad. 59*, 234−238.
43. Shimada, M., Nakatsubo, F., Kirk, T. K., and Higuchi, T. (1981) Biosynthesis of the secondary metabolite veratryl alcohol in relation to lignin degradation by *Phanerochaete chrysosporium*, *Arch. Microbiol. 129*, 321−324.
44. Guillén, F., and Evans, C. S. (1994) Anisaldehyde and veratraldehyde acting as redox cycling agents for H_2O_2 production by *Pleurotus eryngii*, *Appl. Environ. Microbiol. 60*, 2811−2817.
45. de Jong, E., Field, J. A., Dings, J. A. F. M., Wijnberg, J. B. P. A., and de Bont, J. A. M. (1992) De novo biosynthesis of chlorinated aromatics by the white-rot fungus *Bjerkandera* sp BOS55. Formation of 3-chloro-anisaldehyde from glucose, *FEBS Lett. 305*, 220−224.
46. Gutiérrez, A., Caramelo, L., Prieto, A., Martínez, M. J., and Martínez, A. T. (1994) Anisaldehyde production and aryl-alcohol oxidase and dehydrogenase activities in ligninolytic fungi from the genus *Pleurotus*, *Appl. Environ. Microbiol. 60*, 1783−1788.
47. Poulos, T. L., Edwards, S. L., Wariishi, H., and Gold, M. H. (1993) Crystallographic refinement of lignin peroxidase at 2 Å, *J. Biol. Chem. 268*, 4429−4440.
48. Schoemaker, H. E., and Piontek, K. (1996) On the interaction of lignin peroxidase with lignin, *Pure Appl. Chem. 68*, 2089−2096.
49. Ambert-Balay, K., Fuchs, S. M., and Tien, M. (1998) Identification of the veratryl alcohol binding site in lignin peroxidase by site-directed mutagenesis, *Biochem. Biophys. Res. Commun. 251*, 283−286.
50. Gerini, M. F., Roccatano, D., Baciocchi, E., and Di Nola, A. (2003) Molecular dynamics simulations of lignin peroxidase in solution, *Biophys. J. 84*, 3883−3893.
51. Timofeevski, S. L., Nie, G., Reading, N. S., and Aust, S. D. (1999) Addition of veratryl alcohol oxidase activity to manganese peroxidase by site-directed mutagenesis, *Biochem. Biophys. Res. Commun. 256*, 500−504.
52. Smith, A. T., and Doyle, W. A. (2006) Engineered peroxidases with veratryl alcohol oxidase activity, Patent WO/2006/114616.

BI7020298